PLOS COMPUTATIONAL BIOLOGY

RESEARCH ARTICLE

Modeling the efficiency of filovirus entry into cells *in vitro*: Effects of SNP mutations in the receptor molecule

Kwang Su Kim[1☯], **Tatsunari Kondoh**[2☯¤], **Yusuke Asai**[3], **Ayato Takada**[2], **Shingo Iwami**[1,4,5,6*]

1 Department of Biology, Kyushu University, Fukuoka, Japan, **2** Research Center for Zoonosis Control, Hokkaido University, Sapporo, Japan, **3** Disease Control and Prevention Center, National Center for Global Health and Medicine, Tokyo, Japan, **4** MIRAI, Japan Science and Technology Agency, Saitama, Japan, **5** CREST, Japan Science and Technology Agency, Saitama, Japan, **6** Science Groove Inc., Fukuoka, Japan

☯ These authors contributed equally to this work.
¤ Current address: Tatsunari Kondoh: Tsukuba Branch, WDB Co., Ltd., Takezono, Tsukuba, Ibaraki, Japan
* siwami@kyushu-u.org

Citation: Kim KS, Kondoh T, Asai Y, Takada A, Iwami S (2020) Modeling the efficiency of filovirus entry into cells *in vitro*: Effects of SNP mutations in the receptor molecule. PLoS Comput Biol 16(9): e1007612. https://doi.org/10.1371/journal.pcbi.1007612

Editor: Ruy M. Ribeiro, Los Alamos National Laboratory, UNITED STATES

Received: December 14, 2019

Accepted: August 3, 2020

Published: September 28, 2020

Data Availability Statement: All data are available as part of this manuscript and provided in the S1 Data supplemental Excel sheets.

Funding: This study was supported in part by the Basic Science Research Program through the National Research Foundation of Korea funded by the Ministry of Education (2019R1A6A3A12031316 to K.S.K.); JSPS Scientific Research (KAKENHI) B 18KT0018 (to S. I.), 18H01139 (to S.I.), 16H04845 (to S.I.), Scientific Research in Innovative Areas 20H05042

Abstract

Interaction between filovirus glycoprotein (GP) and the Niemann-Pick C1 (NPC1) protein is essential for membrane fusion during virus entry. Some single-nucleotide polymorphism (SNPs) in two surface-exposed loops of NPC1 are known to reduce viral infectivity. However, the dependence of differences in entry efficiency on SNPs remains unclear. Using vesicular stomatitis virus pseudotyped with Ebola and Marburg virus GPs, we investigated the cell-to-cell spread of viruses in cultured cells expressing NPC1 or SNP derivatives. Eclipse and virus-producing phases were assessed by *in vitro* infection experiments, and we developed a mathematical model describing spatial-temporal virus spread. This mathematical model fit the plaque radius data well from day 2 to day 6. Based on the estimated parameters, we found that SNPs causing the P424A and D508N substitutions in NPC1 most effectively reduced the entry efficiency of Ebola and Marburg viruses, respectively. Our novel approach could be broadly applied to other virus plaque assays.

Author summary

Ebola (EBOV) and Marburg (MARV) viruses, which are included viruses of the family Filoviridae, cause severe hemorrhagic fever in humans. Filovirus particles is adsorbed to the cell through glycoprotein (GP), which is the only viral surface protein. Interaction between the filovirus sugar protein (GP) and the Niemann-Pick C1 (NPC1) protein plays a key role in membrane fusion during virus entry. Although some single-nucleotide polymorphism (SNPs) in two surface-exposed loops of NPC1 are known to reduce viral infectivity, the dependence of differences in entry efficiency on SNPs has not been studied. We therefore investigated the cell-to-cell spread of viruses in cultured cells expressing NPC1 or SNP derivatives. Using a mathematical model describing spatial-temporal virus spread, we quantitatively analyze viral entry efficiency and how this affected cell-to-cell spread.

(to S.I.), 19H04839 (to S.I.), 18H05103 (to S.I.); AMED CREST 19gm1310002 (to S.I.); AMED J-PRIDE 18fm0208101 (to A.T.), 19fm0208006s0103, 19fm0208014h0003, and19fm0208019h0103 (to S.I.); AMED Japan Program for Infectious Diseases Research and Infrastructure, 20wm0325007h0001, 20wm0325004s0201, 20wm0325012s0301, 20wm0325015s0301 (to S.I.); AMED Research Program on HIV/AIDS 19fk0410023s0101 (to S.I.); AMED Research Program on Emerging and Re-emerging Infectious Diseases 19fk0108156h0001 and 20fk0108140s0801 (to S.I.); AMED Program for Basic and Clinical Research on Hepatitis 19fk0210036h0502 (to S.I.); AMED Program on the Innovative Development and the Application of New Drugs for Hepatitis B 19fk0310114h0103 (to S.I.); JST MIRAI (to S.I.); Mitsui Life Social Welfare Foundation (to K.W. and S.I.); Shin-Nihon of Advanced Medical Research (to S.I.); Suzuken Memorial Foundation (to S.I.); Life Science Foundation of Japan (to S.I.); SECOM Science and Technology Foundation (to S.I.); The Japan Prize Foundation (to S.I.); Fukuoka Financial Group, Inc. (to S.I.); Kyusyu Industrial Advancement Center Gapfund Program (to S.I.); Foundation for the Fusion of Science and Technology (to S.I.). The funders had no role in study design, data collection and analysis, decision to publish, or preparation of the manuscript.

Competing interests: The authors have declared that no competing interests exist.

Our approach may be applied to not only understanding the roles of genetic polymorphisms in human susceptibility to filoviruses, but also other virus plaque assays.

Introduction

In 2015, the World Health Organization (WHO) included Ebola (EBOV) and Marburg (MARV) viruses among the infectious diseases that should be globally prioritized. Some viruses of the family *Filoviridae*, which includes EBOV and MARV, cause severe hemorrhagic fever in humans and nonhuman primates. In recent years, more frequent filovirus outbreaks have been observed including multiple introductions of filoviruses into the human population, with important implications for worldwide public health [1]

Filovirus particles bear the envelope glycoprotein (GP), which is the only viral surface protein and thus responsible for receptor binding and membrane fusion [2]. Filovirus infection is initiated by binding of GP to attachment factors such as C-type lectins [3, 4], T-cell immunoglobulin and mucin domain 1 (TIM-1) and C-type lectins [5]. Virus particles are internalized into host cells via macropinocytosis and then delivered to late endosomes [6, 7]. GPs are proteolytically processed by cysteine proteases such as cathepsins B and L [8, 9]. This digested GP (dGP) can interact with the host endosomal fusion receptor, Niemann-Pick C1 (NPC1) protein, allowing fusion between the viral envelope and the host endosomal membrane [10, 11]. NPC1 is believed to be essential for filovirus entry into cells [12, 13].

Wang et al. showed that two surface-exposed loops of human NPC1 were important for interaction with dGP and that some amino acid substitutions in these loops reduced binding to dGP [14]. We previously investigated the potential effects of substitutions caused by naturally occurring single-nucleotide polymorphisms (SNPs) in these two loops and found that the P424A/D508N and S425L/D502E substitutions in human NPC1 reduced entry of vesicular stomatitis virus (VSV) pseudotyped with EBOV and MARV GPs, respectively [7]. We also found that the plaque sizes of replication-competent VSVs bearing EBOV and MARV GPs (VSV*Δ*G-EBOV and VSV*Δ*G-MARV) were reduced. However, it remains unclear how these SNPs and associated substitutions influence the spread of the viruses in plaque assays. In general, plaque formation is affected by multiple processes including cell-to-cell infection, viral production time, latent time, and intracellular replication. Because of this complexity, it is difficult to quantitatively understand the kinetics of viral infection. Although various modeling approaches have been studied for quantitative analysis of viral infections [15–18], a new modeling approach is needed that accurately corresponds to experiments performed to quantitatively measure only entry efficiency affected by SNPs.

In this study, we focused on the interaction between GP and NPC1, enabling us to estimate the cellular entry efficiency during plaque formation of VSV*Δ*G-EBOV and VSV*Δ*G-MARV. We employed viral infection assays combined with mathematical analyses as described previously [15–17, 19] to quantitatively analyze viral entry efficiency and how this affected cell-to-cell spread. We found that the P424A and S425L substitutions reduced the entry efficiency of VSVΔG-EBOV by 47% and 21%, respectively, while the other SNPs and substitutions did not affect entry (reduction of $<16\%$). Furthermore, we showed that our mathematical model recapitulates the process of merging viral plaques. This method could also be applied to plaque assays for other viruses and could be used to improve *in vitro* determination of the effects of mutations on viruses and target cells.

Results

Distribution of infectious phases of VSVΔG-EBOV and VSVΔG-MARV

We assumed that amino acid mutations of the cellular NPC1 protein only changed virus entry efficiency; the eclipse phase and infectious phase remained unchanged. To estimate the infectious phase for VSVΔG-EBOV and VSVΔG-MARV, we performed virus production assays using Vero E6/NPC1-KO cells expressing human NPC1 (293T-NPC1) (**Fig 1A and 1B**, left panels; see also **Methods**). In three of the four experiments (Exp1, 3, and 4), VSVΔG-EBOV-inoculated cells started to produce infectious virus particles at 6 h post inoculation. In Exp2, the inoculated cells started to produce virus at 9 h post-inoculation. The virus-producing cells died by 33 h post-inoculation in all experiments. Thus, we assumed that infected cells which produce infectious viruses are in "infectious phase". In our experiments, since the discrepancy in virus production time was 3 h and the exact virus production time was unknown, candidate groups were classified as follows: candidates for the time when infected cells begin to produce virus were 4, 5, and 6 h (occurring in three instances), while candidates at 7, 8, and 9 h occurred only once. In all four experiments, the death of all infected cells was observed at 33 h post-inoculation. This suggested that the candidates for time of cell death were 31, 32, and 33 h, and if we consider the above virus production start time, the infectious phase was between 22 and 29 h in duration. By contrast, for VSVΔG-MARV-inoculated cells, the infectious phase was between 25 and 29 h in duration.

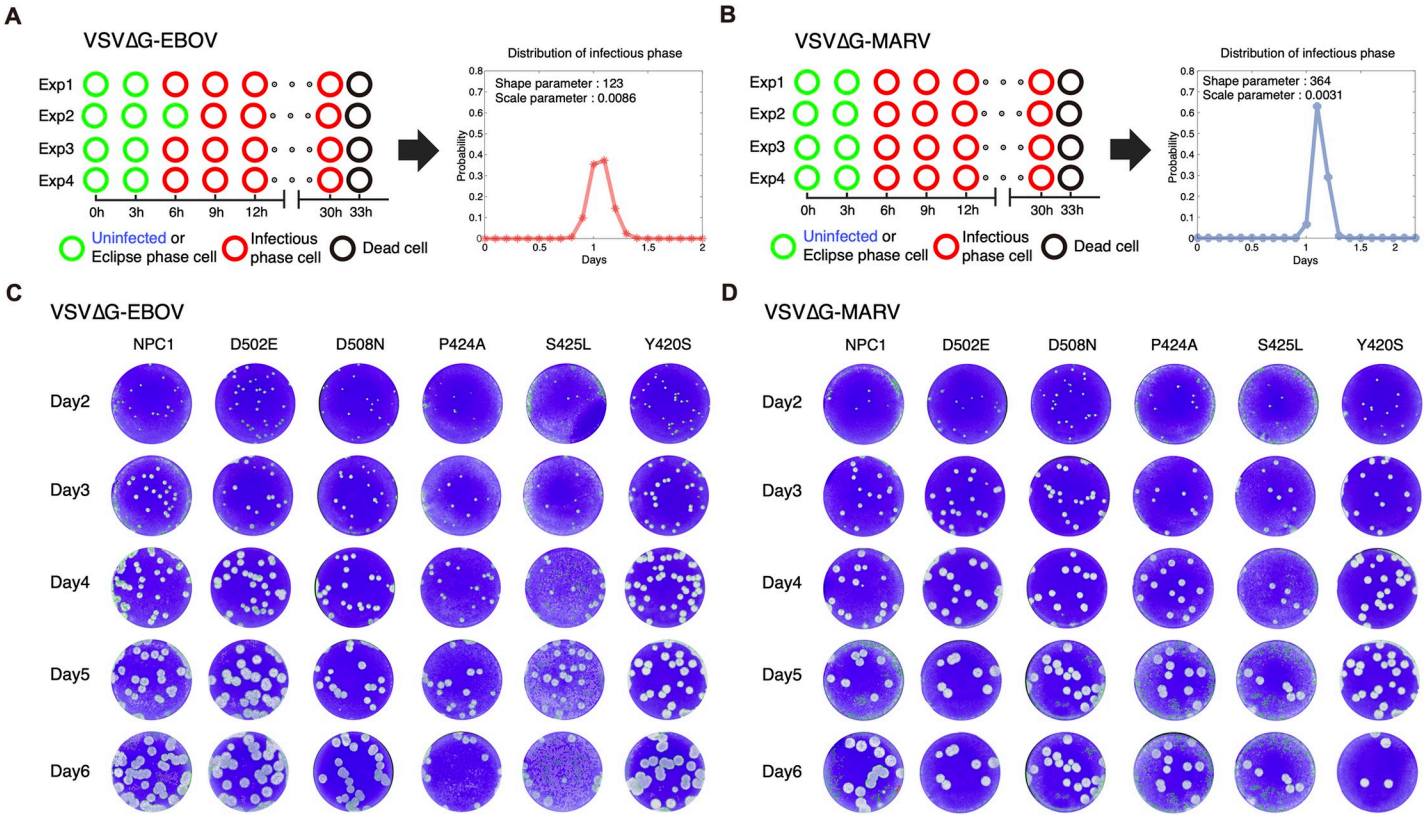

Fig 1. Virus production assays and plaque assays. Virus production assays using Vero E6/NPC1-KO cells expressing human NPC1. Four independent experiments recording cell state every 3 h for VSVΔG-EBOV and VSVΔG-MARV are shown in the left panels of **(A)** and **(B)**, respectively. Estimated distributions of the infectious phases of each are is also shown in the right panel. Plaque formation of VSVΔG-EBOV **(C)** and VSVΔG-MARV **(D)** on Vero E6 cells expressing wildtype NPC1 and five SNP mutants on days 2–6 are shown. Gray spots represent plaques formed by dead cells.

https://doi.org/10.1371/journal.pcbi.1007612.g001

Because the infectious phase was relatively long compared with the duration of the eclipse phase, we assumed that the infectious phase follows the Erlang distribution which is a multiexponential case of the gamma distribution as described previously [20, 21]. The equivalence between the expression for, and the parameters of, the probability density functions of the Erlang distributions is shown as follows [22]:

$$f(a) = \frac{a^{\gamma-1}}{\Gamma(\gamma)\eta^{\gamma}} e^{-\frac{a}{\eta}} \sim \frac{a^{n_I-1}}{(n_I-1)!\left(\frac{\tau_I}{n_I}\right)^{n_I}} e^{-\frac{a}{(\tau_I/n_I)}}$$

The shape ($\gamma = n_I = 123$ and 364) and scale ($\eta = \tau_I/n_I = 8.64\times10^{-3}$ and 3.10×10^{-3}) parameters of the Erlang distribution for VSVΔG-EBOV and VSVΔG-MARV were estimated by fitting the candidates for the infectious phase, respectively (**Table 1**). Note that n_I and τ_I correspond to the number of "subdivided" compartments and the average duration of the infectious phase, respectively, in Eq (4) [21, 22] (see later). The probability density functions of the estimated Erlang distributions of infectious phases are shown in the right panels of **Fig 1A and 1B**. Conversely, we assumed that the eclipse phase with relatively short duration follows an exponential distribution as in many basic virus dynamics models [23–25]. We planned to quantify the eclipse phase for VSVΔG-EBOV and VSVΔG-MARV from the results of plaque assays together with other parameters (see later).

Spatial-temporal mathematical model for viral plaque amplification

To quantify and compare the filovirus entry efficiency among cells expressing wildtype and SNP-mutant NPC1, we performed viral plaque assays using cells expressing wildtype NPC1 (293T-NPC1) and five SNP mutants for VSVΔG-EBOV and VSVΔG-MARV (**Fig 1C and 1D**). The viral plaque is considered as the area formed by dead cells, and thus the plaque radius is defined by the distance from the center of plaque to its edge. We measured the average sizes of independent plaques (see **Methods**) and used them to quantify spatial-temporal VSVΔG-EBOV and VSVΔG-MARV spread. First, we developed a novel mathematical model for viral plaque amplification as follows. Because monolayers of cells were overlaid with agar media in our plaque assay, there was no cell movement. Only cell-to-cell infections between infected and adjacent uninfected cells occur. We assumed that the inner infected cell infects only adjacent outer target cells (**Fig 2A**). To describe the infection dynamics of virus in the plate, we derived the following mathematical model including two independent variables (time t and

Table 1. Parameter values estimated from plaque assay and virus production assay.

Parameter Name	Symbol	Unit	Virus type	Wildtype	D502E	D508N	P424A	S425L	Y420S
Number of subdivided compartments	n_I	—	VSVΔG-EBOV	123					
			VSVΔG-MARV	364					
Length of infectious phase	τ_I	day	VSVΔG-EBOV	1.06					
			VSVΔG-MARV	1.13					
Rate constant for infections	ω	(cell· day)$^{-1}$	VSVΔG-EBOV	0.38					
			VSVΔG-MARV	0.41					
Length of eclipse phase	$1/k$	day	VSVΔG-EBOV	0.19					
			VSVΔG-MARV	0.22					
Initial radius of viral plaque	r_0	mm	VSVΔG-EBOV	0.23					
			VSVΔG-MARV						
Relative virus entry efficiency	α	—	VSVΔG-EBOV	1.00	1.26	0.84	0.53	0.79	1.05
			VSVΔG-MARV	1.00	1.12	0.93	1.1	1.05	1.15

https://doi.org/10.1371/journal.pcbi.1007612.t001

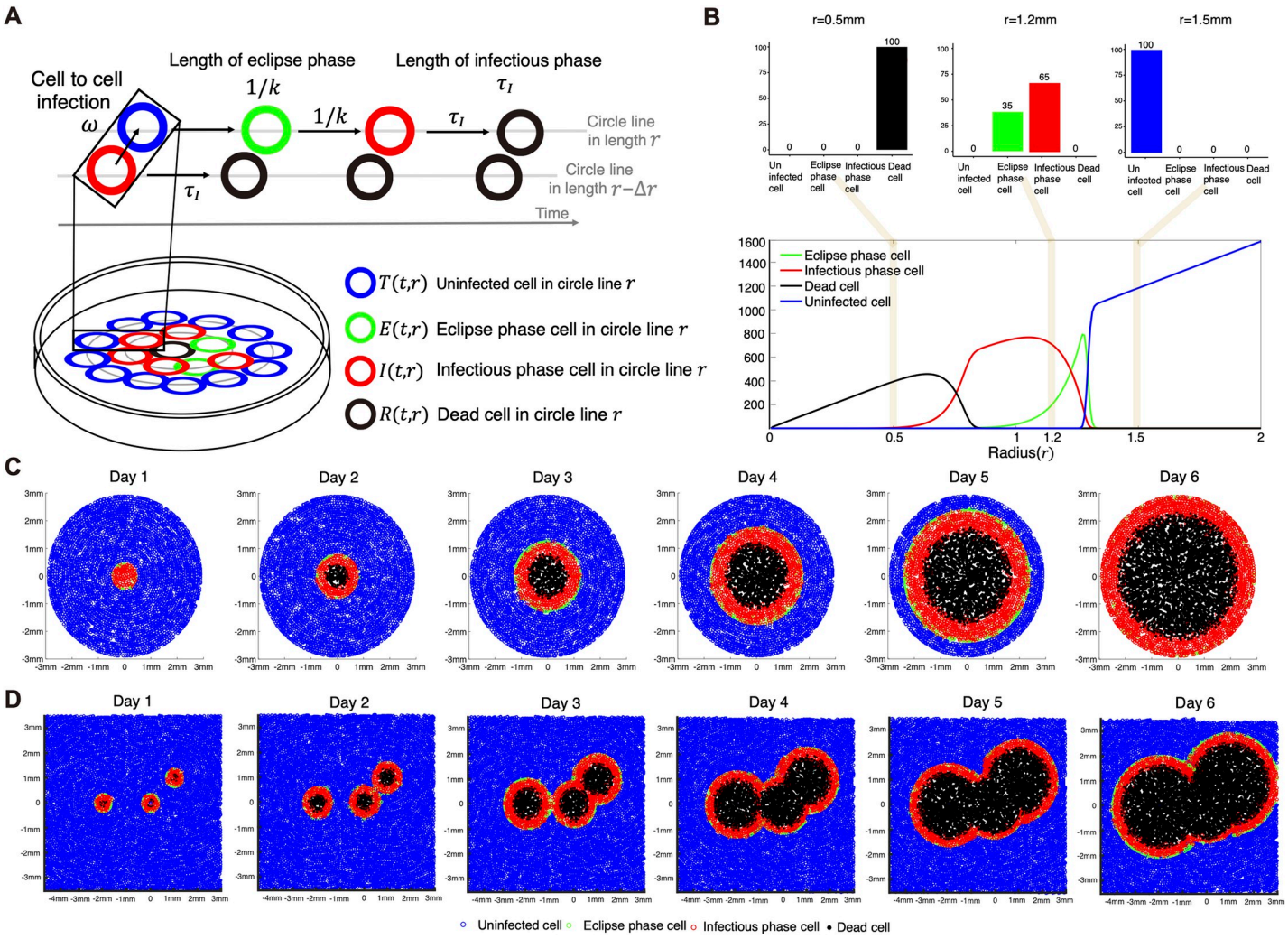

Fig 2. Modeling and visualizing viral plaque amplification. Modeling spatial-temporal dynamics of viral plaque amplification is shown in **(A)**. A representative simulation for plaque amplification on day 3 is shown in **(B)**. The ratio of cells for each radius (e.g., 0.5mm, 1.2mm and 1.5mm) can be calculated in the top panels. In **(C)**, a representation of a single viral plaque amplification is described for each day. Merging of three plaques can be also described by considering overlapping portions over time in **(D)**.

https://doi.org/10.1371/journal.pcbi.1007612.g002

radius of circle r) and four state variables (uninfected, eclipse phase, infectious phase and dead cells):

$$\frac{dT(t,r)}{dt} = -\alpha\omega T(t,r)\sum_{j=1}^{n_I} I_j(t,r-\Delta r), \tag{1}$$

$$\frac{dE(t,r)}{dt} = \alpha\omega T(t,r)\sum_{j=1}^{n_I} I_j(t,r-\Delta r) - kE(t,r), \tag{2}$$

$$\frac{dI_1(t,r)}{dt} = kE(t,r) - \frac{n_I}{\tau_I} I_1(t,r), \tag{3}$$

$$\frac{dI_{j=2,\ldots,n_I}(t,r)}{dt} = \frac{n_I}{\tau_I} I_{j-1}(t,r) - \frac{n_I}{\tau_I} I_j(t,r), \tag{4}$$

$$\frac{dD(t,r)}{dt} = \frac{n_I}{\tau_I} I_{n_I}(t,r). \tag{5}$$

The initial conditions were: $I_1(0,r) = 2\pi \times r/0.008$ for $r \leq r_0$ and 0 for $r > r_0$, $T(0,r) = 0$ for $r \leq r_0$ and $2\pi \times r/0.008$ for $r > r_0$, and $E(0,r) = D(0,r) = 0$ for $r > 0$. Here $T(t,r)$, $E(t,r)$, $I_j(t,r)$ and $D(t,r)$ represent the numbers of uninfected, eclipse phase, infectious phase and dead cells, respectively. Note that Eq (4) is derived from the following integro-differential equation by "linear-chain-trick":

$$I_j(t,r) = \int_0^\infty \frac{a^{n_I-1}}{(n_I-1)!\left(\frac{\tau_I}{n_I}\right)^{n_I}} e^{-\frac{a}{(\tau_I/n_I)}} kE(t-a,r)da.$$

The linear chain trick is method to change from continuous-time stochastic state transition model in which an individual's time spent in a given state lasts to ODE models [26]. This method allows us to only represent not delayed infectious phase state but also applicable for numerical simulation [18, 27, 28]. In the integro-differential equation, the shape parameter n_I represent equation number in Eq (4). We also assumed that infectious cells of the I_1 compartment were inoculated only in a radius of less than r_0 and there were no other infected cells at the initial time. In the Eqs (1) and (2), the term $(\alpha\omega T(t,r) \sum_{j=1}^{n_I} I_j(t, r-\Delta r))$ represents a process that the target cell located at circle line of radius (r) is infected by infected cells located at circle line of radius (r–Δr). The parameters ω and $1/k$ represent the infection rate of cells expressing 293T-NPC1 and the length of the eclipse phase, respectively, and thus α is the relative virus entry efficiency into target cells bearing amino acid mutations in the cellular NPC1 (i.e., we fixed $\alpha = 1$ for 293T-NPC1-expressing cells). Values of entry efficiency (α) larger than 1 means shorter the virus entry time and more efficient infection of uninfected cells.

Simulating and visualizing viral plaque amplification

The number of target cells in our plate was initially distributed as follows. The radius of the plate was 17.35 mm and the average cell radius was 0.004 mm. This implies that there are 17.35 mm/0.008 mm = 2169 circle lines in which cells are distributed in the plate. If the circumference of the circle line is divided by the diameter of the cell, we can obtain the number of cells distributed in one circle line of radius r, that is, $2\pi r/0.008$. Since the radius of each circle line increases proportionally to the cell interval (0.008 mm), total cell number in the plate can be calculated as $\sum_{i=1}^{2169} 2\pi \times 0.008 \times i/0.008 = 1.779 \times 10^7$, and was consistent with the number of cells used in our experiments.

Using a finite difference method, we computed a numerical solution of Eqs (1–5) with respect to time t and circle radius r in the plate. In the bottom panel of **Fig 2B**, for example, the distribution of each cell according to the radius at day 3 is shown. Dead cells (black line) are located at a radius of 0.8 mm from the center of the plaque which is considered as "a plaque radius" in our simulation. That is, we defined the simulated viral plaque radius as the length of a plaque from its center to the edge of dead cells in the plaque. Here the edge is defined as the first circle line which does not include any dead cell (dead cells fewer than "1" were not counted). Infectious cells (red line) are distributed from 0.5 to 1.3 mm in radius, and eclipse phase cells (green line) gradually increase as the radius increases, peaking at 1.3 mm. This

differs from the distribution of infectious cells in the wide radius region because the time spent in the infectious phase is relatively longer than the time spent in the eclipse phase. Although we assumed any cells in an inner circle line can interact with those in the adjacent outer circle line, our mathematical model, Eqs (1–5), can describe virus amplification in the plaque which is a minimum model for quantitatively analyzing "plaque size" (see later).

Next, to visualize amplification of an average viral plaque, we calculated the percentage of cells corresponding to each state with respect to time t and circle radius r based on Eqs (1–5). For example, in the top panels of **Fig 2B**, the corresponding percentage of each cell at radius 0.5 mm, 1.2 mm and 1.5 mm on day 3 is shown. There were only dead cells at radius 0.5 mm. At radius 1.2 mm (depicted in the second bar graph), eclipse phase and infectious phase cells comprised 35% and 65% of cells, respectively. Only uninfected cells were present at radius 1.5 mm, as infection had not yet occurred. After calculating the ratio of cells at each radius, we chose each cell state depending on the ratio at a circle line by line. By simulation over time, in **Fig 2C**, we show a representation of viral plaque amplification. On day 1, no plaque has yet been generated; only uninfected cells, infectious cells and eclipse phase cells are distributed. On day 2, a plaque of dead cells is forming (black circle). The eclipse phase cells, which are represented by a green circle, are narrowly distributed on the edge of the infectious cell area, and the infectious cells are in turn distributed in the wide radius region because the period spent in the infectious phase is longer than that in the eclipse phase as explained above. Note that in **Fig 2C**, we show only the change of composition within the area inside a 3-mm radius, not the whole plate. All uninfected cells disappear inside this radius, and only infectious cells and dead cells remain at day 6.

In the plaque assay data for day 6 in **Fig 1C and 1D**, we can see that several plaques expanded to form a larger contiguous plaque. We demonstrated that Eqs (1–5) can reproduce these merging plaques (see detail in **S1 Text**). In **Fig 2D**, the dynamics of the merging three plaques located at different positions are shown as snapshots. In **S1 and S2 Movies**, we also showed how two and three plaques merge in a spatial-temporal manner.

Quantifying filovirus entry efficiency for cellular NPC1 SNP mutations

The plaque radii generated by infection of wildtype and mutant NPC1-expressing cells were measured and compared with fitting results of the radius of viral plaques simulated by Eqs (1–5) for the six amino acid mutations in both viruses, as shown in **Fig 3A** (see also Methods). For all of the NPC1 mutants, the plaque radius for VSVΔG-EBOV was smaller than that for VSVΔG-MARV, meaning that the infectivity (i.e., entry efficiency) of VSVΔG-MARV was greater than that of VSVΔG-EBOV, regardless of the sequence of NPC1. The estimated parameter values are shown in **Table 1** and the viral entry efficiency, α, is shown in **Fig 3B**. In the case of VSVΔG-MARV, the entry efficiencies into wildtype and mutant NPC1-expressing cells were similar. Indeed, the entry efficiencies of NPC1 mutants were slightly greater than that of 293T-NPC1 except for the D508N and Y420S substitutions, which had the highest entry efficiency (15% above wildtype). In the case of VSVΔG-EBOV, the P424A, S425L, and D508 substitutions in NPC1 resulted in lower entry efficiencies than 293T-NPC1. The P424A substitution showed the lowest entry efficiency (47% reduction compared with 293T-NPC1). In contrast, the D502E substitution, which had the highest entry efficiency among the NPC1 mutants for VSVΔG-EBOV, demonstrated 26% higher entry efficiency than wildtype NPC1 (discussed below).

Discussion

In general, plaque formation is affected by multiple processes including viral entry, membrane fusion, genome replication, transportation, and virion assembly efficiency. Because of this

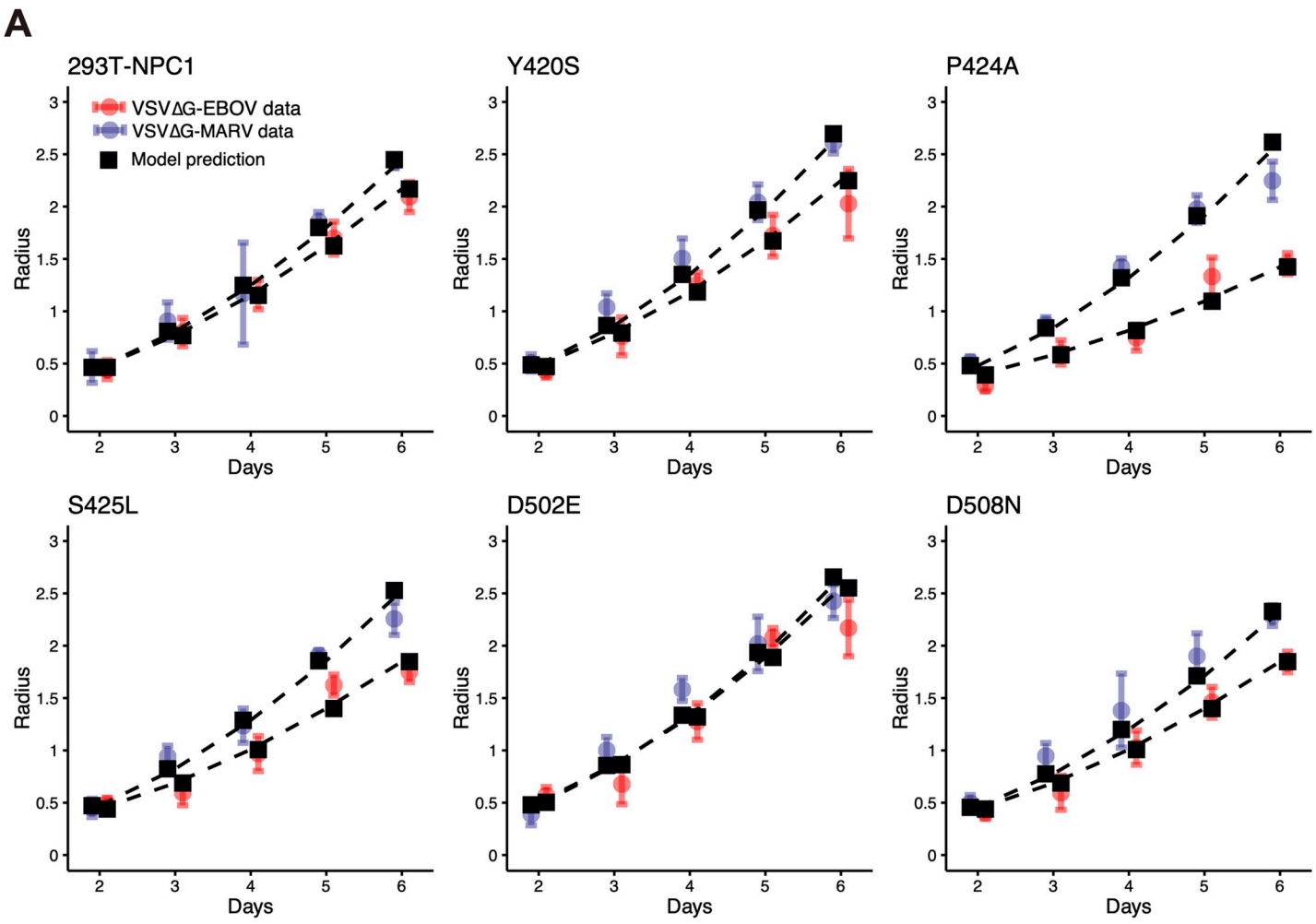
A
293T-NPC1
Y420S
P424A
S425L
D502E
D508N
VSVΔG-EBOV data
VSVΔG-MARV data
Model prediction
Radius
Days

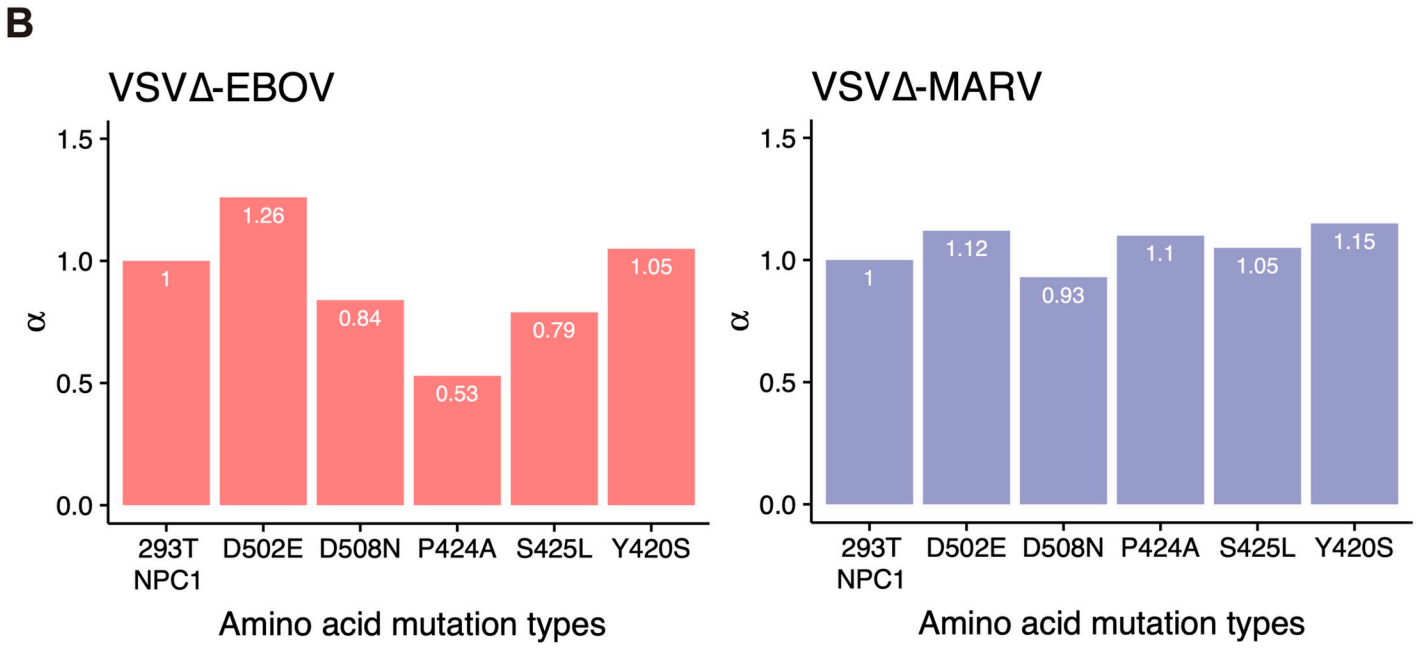
B
VSVΔ-EBOV
VSVΔ-MARV
α
1
1.26
0.84
0.53
0.79
1.05
1.12
0.93
1.1
1.05
1.15
293T NPC1
D502E
D508N
P424A
S425L
Y420S
Amino acid mutation types

Fig 3. Quantifying VSVΔG-EBOV and VSVΔG-MARV entry efficiency for different NPC1 SNPs. Fits of the mathematical model, Eqs (1–5), to the experimental data of VSVΔG-EBOV and VSVΔG-MARV in plaque assays are shown in **(A)**. Black squares represent plaque radii from simulations with best-fit parameters for each SNP. Blue and red circles and bars represent the means and standard deviations of the plaque radii following VSVΔG-EBOV and VSVΔG-MARV infection, respectively, on wildtype and mutant NPC1-expressing cells. Compared with infection of 293T-NPC1-expressing cells by VSVΔG-EBOV and VSVΔG-MARV, relative entry efficiency, α, fitting the plaque radius dataset was estimated for each NPC1 SNP and shown in **(B)**.

https://doi.org/10.1371/journal.pcbi.1007612.g003

complexity, it is difficult to quantitatively understand the kinetics of viral infection and how the efficiency of entry is affected by individual SNPs. Moreover, the time course of plaque data is challenging to understand intuitively. Additionally, there is no experimental technique available to measure only entry efficiency as an absolute value excluding other causes of viral spread. To address this point, we employed two viral infection assays (i.e., plaque-forming assay and virus production assay) combined with mathematical analyses to quantitatively analyze how particular SNPs affected virus entry. Previous mathematical models which describe plaque expansion considered the diffusion of virus [29–32], but under our experimental conditions, the infected cells were overlaid with agar and thus only cell-to-cell infection was monitored. Agent-based models can describe spatially explicit mechanisms [33, 34]. However, these approaches are difficult to directly fit to plaque radius data in a time course manner. A model including the infection term for the decreasing proportion of cells contributing to cell-to-cell was also suggested [35]. In recent paper by Graw et al. [36], with liver biopsy samples of patients, they characterized the cluster structures of infected cells using intracellular HCV RNA replication model. They applied statistical methods to investigate properties of clusters of infected cells while we applied the modeling spatial-temporal dynamics to characterize plaque formations.

We developed a simple but well approximated mathematical model, i.e., Eqs (1–5), that can analyze plaque assay data with minimal assumptions to quantitatively compare and analyze the virus entry efficiency by focusing on the interactions between GP and NPC1. VSVΔG-EBOV and VSVΔG-MARV usually grow in cultured cells as well as VSV (taking several hours to produce cytopathic effect (CPE)), whereas EBOV and MARV do not grow as rapidly as VSV. These pseudotyped VSVs enabled us to concentrate on the interaction between GP and NPC1 without considering other factors, since all other viral proteins are identical between VSVΔG-EBOV and VSVΔG-MARV. Thus, we could evaluate entry efficiency and objectively compare each SNP after parameterization by Eqs (1–5) for VSVΔG-EBOV and VSVΔG-MARV. The entry efficiencies of VSVΔG-MARV in cells expressing NPC1 with different SNPs and substitutions ranged from −7% to +15% compared with 293T-NPC1 (wild-type human NPC1), while the efficiencies of VSVΔG-EBOV showed relatively large changes ranging from −47% to +26%. These results indicated that the entry efficiency of VSVΔG-EBOV was more sensitive to changes in NPC1 sequence. Notably, the P424A and S425L substitutions reduced the entry efficiency of VSVΔG-EBOV by 47% and 21%, respectively, but only reduced the entry efficiency of VSVΔG-MARV by 10% and 5%, respectively. This supports the possibility that the P424A and S425L substitutions have different effects due to differences between Ebola and Marburg viruses observed in previous studies [37]. The D508N substitutions reduced entry efficiency for both Ebola and Marburg viruses. We found that P424A and D508N substitutions significantly reduced the entry of VSVΔG-EBOV. Although it might be difficult to completely apply the values determined here for entry efficiency to *bona fide* EBOV and MARV infection, our result is consistent with previous investigations [37]. We highlight that pseudotyped viruses are useful in mathematical model-based quantitative data analyses focusing on a specific molecular interaction. For example, if we polymerase mutations into EBOV and MARV, similar approach might reveal the differences in viral replication efficiency

and their dependence on mutations. Our novel approach could be broadly applied to other virus plaque assays.

Through this experimental-mathematical investigation, we quantified the entry efficiency of VSVΔG-EBOV and VSVΔG-MARV based on cell-to-cell spread during plaque formation and found differences among cells bearing SNPs and amino acid substitutions in the filovirus receptor (i.e., NPC1). Although there have been some studies of asymptomatic filovirus infection [38, 39], the mechanisms through which individuals appear to be inherently resistant to EBOV and MARV have not yet been understood. It will be of interest to investigate NPC1 variation and its influence on EBOV and MARV entry efficiency and also to identify genetic backgrounds that affect the susceptibility of humans to filovirus infection, both of which will provide important information for understanding filovirus disease progression and host restriction. Combining *in vitro* experiments and mathematical models gradually provides detailed quantitative insights into the kinetics of virus infection [17, 40, 41]. Thus, our method may also be applied to understanding the roles of genetic polymorphisms in human susceptibility to filoviruses.

Methods

Viruses and cells

Replication-competent recombinant VSVs pseudotyped with EBOV (Mayinga) and MARV (Angola) GPs (VSV*Δ*G-EBOV and VSV*Δ*G-MARV, respectively) were generated as described previously [42]. VSV*Δ*G-EBOV and VSV*Δ*G-MARV were propagated in Vero E6 cells and stored at -80˚C until use. Infectivity of the viruses in each cell line was determined by a plaque-forming assay as described previously [43]. All work using these viruses was performed in the BSL-3 laboratories at the Research Center for Zoonosis Control, Hokkaido University, Japan. Vero E6 cells (ATCC CRL-1586), NPC1-knockout Vero E6 (Vero E6/NPC1-KO), and Vero E6 cell lines stably expressing each NPC1 SNP (293T-NPC1, Y420S, P424A, S425L, D502E, D508N) [7] substitution were grown in Dulbecco's modified Eagle's medium (DMEM, Sigma) supplemented with 10% fetal calf serum (FCS).

Plaque assay

VSV*Δ*G-EBOV and VSV*Δ*G-MARV (multiplicity of infection, MOI = 0.0005 in Vero E6 cells) were inoculated onto monolayers of each cell line in six-well tissue culture plates (Corning). After adsorption for 1 h, the inoculum was completely removed, and the cells were overlaid with Eagle's minimal essential medium containing 1.0% Bacto Agar (BD) and then incubated for 2–6 days at 37˚C. Cells were stained with 0.5% crystal violet in 10% formalin at 24 h intervals. Plaque images in the wells were captured and each plaque size (mm^2) was measured using a CTL-ImmunoSpot S6 Macro Analyzer equipped with ImmunoCapture ver. 6.5 and BioSpot 5.0 software (Cellular Technology Ltd. USA). We examined all plaques which were completely separated from one another. Average sizes of independent plaques were used for mathematical model-based quantitative data analyses.

Virus production assay

Vero E6 cells grown in 96-well tissue culture plates (Corning) were inoculated with VSV*Δ*G-EBOV and VSV*Δ*G-MARV (MOI = 1.0). After adsorption for 1 h, the inoculum was completely removed. One hundred microliters of growth medium (DMEM supplemented with 10% FCS) were added into each well and then incubated for 33 h at 37˚C. Supernatants of the culture medium were collected at 3 h intervals and frozen at -80˚C until use. To check the presence of

infectious virus particles in the collected supernatants, confluent monolayers of Vero E6 cells on 96-well tissue culture plates (Corning) were inoculated with the supernatant collected at each time point. After incubation for 3 days at 37˚C, virus infection was assessed by the presence of CPE. This assay enabled us to predict the time when infected cells shift from non-virus-producing to virus-producing cells (i.e., eclipse phase).

Data fitting and parameter estimation

Because the number of experimental measured plaques and the radius of each plaque were different (we simply employed the mean radius of plaques which had not merged), we used in our data fitting the weighted least square method considering the means and standard deviations of the observations, $\mathrm{SSR} = \sum_{i=2}^{6} (D_i - M_i)^2/\mathrm{SD}_i^2$, where D_i and SD_i are the mean and standard deviation of the plaque radius in experiments, respectively, and M_i is the radius of the plaque in our simulation at day i = 2,3,. . .,6. Using estimated τ_I and n_I in the virus production assay, we estimated the parameters ω and k for VSVΔG-EBOV and VSVΔG-MARV, and the common initial value of r_0 from the plaque assay with 293T-NPC1. With these estimated parameters, we quantified the viral entry efficiency, α, for VSVΔG-EBOV and VSVΔG-MARV from the plaque assay with amino acid mutations in NPC1 (D502E, D508N, P424A, S425L and Y420S). All estimated parameters are summarized in **Table 1** and **Fig 3B**.

Supporting information

S1 Text. Simulation of merging viral plaques.
(DOCX)

S1 Fig. Ratio of plaque overlap during plaque merging.
(DOCX)

S1 Movie. Spatial-temporal dynamics of two plaques merging.
(AVI)

S2 Movie. Spatial-temporal dynamics of three plaques merging.
(AVI)

S1 Data. Experimental data sets for Fig 3A.
(XLSX)

Author Contributions

Conceptualization: Shingo Iwami.

Data curation: Tatsunari Kondoh, Ayato Takada.

Formal analysis: Kwang Su Kim, Shingo Iwami.

Writing – original draft: Kwang Su Kim, Tatsunari Kondoh, Ayato Takada, Shingo Iwami.

Writing – review & editing: Kwang Su Kim, Tatsunari Kondoh, Yusuke Asai, Ayato Takada, Shingo Iwami.

References

1. WHO. Ebola virus disease 2019, March 3. Available from: https://www.who.int/en/news-room/fact-sheets/detail/ebola-virus-disease.

2. Takada A, Robison C, Goto H, Sanchez A, Murti KG, Whitt MA, et al. A system for functional analysis of Ebola virus glycoprotein. Proc Natl Acad Sci U S A. 1997; 94(26):14764–9. Epub 1998/02/07. https://doi.org/10.1073/pnas.94.26.14764 PMID: 9405687; PubMed Central PMCID: PMC25111.

3. Hofmann-Winkler H, Kaup F, Pohlmann S. Host cell factors in filovirus entry: novel players, new insights. Viruses. 2012; 4(12):3336–62. Epub 2013/01/25. https://doi.org/10.3390/v4123336 PMID: 23342362; PubMed Central PMCID: PMC3528269.

4. Takada A. Filovirus tropism: cellular molecules for viral entry. Front Microbiol. 2012; 3:34. Epub 2012/03/01. https://doi.org/10.3389/fmicb.2012.00034 PMID: 22363323; PubMed Central PMCID: PMC3277274.

5. Kondratowicz AS, Lennemann NJ, Sinn PL, Davey RA, Hunt CL, Moller-Tank S, et al. T-cell immunoglobulin and mucin domain 1 (TIM-1) is a receptor for Zaire Ebolavirus and Lake Victoria Marburgvirus. Proc Natl Acad Sci U S A. 2011; 108(20):8426–31. Epub 2011/05/04. https://doi.org/10.1073/pnas.1019030108 PMID: 21536871; PubMed Central PMCID: PMC3100998.

6. Nanbo A, Imai M, Watanabe S, Noda T, Takahashi K, Neumann G, et al. Ebolavirus is internalized into host cells via macropinocytosis in a viral glycoprotein-dependent manner. PLoS Pathog. 2010; 6(9):e1001121. Epub 2010/10/05. https://doi.org/10.1371/journal.ppat.1001121 PMID: 20886108; PubMed Central PMCID: PMC2944813.

7. Saeed MF, Kolokoltsov AA, Albrecht T, Davey RA. Cellular entry of ebola virus involves uptake by a macropinocytosis-like mechanism and subsequent trafficking through early and late endosomes. PLoS Pathog. 2010; 6(9):e1001110. Epub 2010/09/24. https://doi.org/10.1371/journal.ppat.1001110 PMID: 20862315; PubMed Central PMCID: PMC2940741.

8. Chandran K, Sullivan NJ, Felbor U, Whelan SP, Cunningham JM. Endosomal proteolysis of the Ebola virus glycoprotein is necessary for infection. Science. 2005; 308(5728):1643–5. Epub 2005/04/16. https://doi.org/10.1126/science.1110656 PMID: 15831716; PubMed Central PMCID: PMC4797943.

9. Misasi J, Chandran K, Yang JY, Considine B, Filone CM, Cote M, et al. Filoviruses require endosomal cysteine proteases for entry but exhibit distinct protease preferences. J Virol. 2012; 86(6):3284–92. Epub 2012/01/13. https://doi.org/10.1128/JVI.06346-11 PMID: 22238307; PubMed Central PMCID: PMC3302294.

10. Cote M, Misasi J, Ren T, Bruchez A, Lee K, Filone CM, et al. Small molecule inhibitors reveal Niemann-Pick C1 is essential for Ebola virus infection. Nature. 2011; 477(7364):344–U122. https://doi.org/10.1038/nature10380 PubMed PMID: WOS:000294852400034. PMID: 21866101

11. Simmons G. Filovirus Entry. Adv Exp Med Biol. 2013; 790:83–94. doi: Book_Doi https://doi.org/10.1007/978-1-4614-7651-1_5 PubMed PMID: WOS:000332631900006. PMID: 23884587

12. Herbert AS, Davidson C, Kuehne AI, Bakken R, Braigen SZ, Gunn KE, et al. Niemann-Pick C1 Is Essential for Ebolavirus Replication and Pathogenesis In Vivo. Mbio. 2015; 6(3). doi: ARTN e00565-15. https://doi.org/10. 1128/mBio.00565-15 PubMed PMID: WOS:000357867400050.

13. Li XC, Saha P, Li J, Blobel G, Pfeffer SR. Clues to the mechanism of cholesterol transfer from the structure of NPC1 middle lumenal domain bound to NPC2. P Natl Acad Sci USA. 2016; 113(36):10079–84. https://doi.org/10.1073/pnas.1611956113 PubMed PMID: WOS:000383094500042. PMID: 27551080

14. Wang H, Shi Y, Song J, Qi JX, Lu GW, Yan JH, et al. Ebola Viral Glycoprotein Bound to Its Endosomal Receptor Niemann-Pick C1. Cell. 2016; 164(1–2):258–68. https://doi.org/10.1016/j.cell.2015.12.044 PubMed PMID: WOS:000368339300025. PMID: 26771495

15. Perelson AS, Essunger P, Cao YZ, Vesanen M, Hurley A, Saksela K, et al. Decay characteristics of HIV-1-infected compartments during combination therapy. Nature. 1997; 387(6629):188–91. https://doi.org/10.1038/387188a0 PubMed PMID: WOS:A1997WX94500056. PMID: 9144290

16. Iwami S, Sato K, De Boer RJ, Aihara K, Miura T, Koyanagi Y. Identifying viral parameters from in vitro cell cultures. Front Microbiol. 2012; 3. doi: ARTN 319. https://doi.org/103389/fmicb.2012.00319 PubMed PMID: WOS:000208863600324.

17. Iwami S, Takeuchi JS, Nakaoka S, Mammano F, Clavel F, Inaba H, et al. Cell-to-cell infection by HIV contributes over half of virus infection. Elife. 2015; 4. Epub 2015/10/07. https://doi.org/10.7554/eLife.08150 PMID: 26441404; PubMed Central PMCID: PMC4592948.

18. Kakizoe Y, Nakaoka S, Beauchemin CAA, Morita S, Mori H, Igarashi T, et al. A method to determine the duration of the eclipse phase for in vitro infection with a highly pathogenic SHIV strain. Sci Rep-Uk. 2015; 5. doi: ARTN 10371. https://doi.org/10.1128/mBio.00565-15 PubMed PMID: WOS:000357867400050. PMID: 26015498

19. Iwanami S, Kakizoe Y, Morita S, Miura T, Nakaoka S, Iwami S. A highly pathogenic simian/human immunodeficiency virus effectively produces infectious virions compared with a less pathogenic virus in cell culture. Theor Biol Med Model. 2017; 14. doi: ARTN 9. https://doi.org/101186/s12976-017-0055-8 PubMed PMID: WOS:000400138900001.

20. Beauchemin CAA, Miura T, Iwami S. Duration of SHIV production by infected cells is not exponentially distributed: Implications for estimates of infection parameters and antiviral efficacy. Sci Rep-Uk. 2017; 7. doi: ARTN 42765. https://doi.org/10. 1038/srep42765 PubMed PMID: WOS:000394208700001

21. Pinilla LT, Holder BP, Abed Y, Boivin G, Beauchemin CA. The H275Y neuraminidase mutation of the pandemic A/H1N1 influenza virus lengthens the eclipse phase and reduces viral output of infected cells, potentially compromising fitness in ferrets. J Virol. 2012; 86(19):10651–60. Epub 2012/07/28. https://doi.org/10.1128/JVI.07244-11 PMID: 22837199; PubMed Central PMCID: PMC3457267.

22. Kakizoe Y, Nakaoka S, Beauchemin CA, Morita S, Mori H, Igarashi T, et al. A method to determine the duration of the eclipse phase for in vitro infection with a highly pathogenic SHIV strain. Scientific reports. 2015; 5:10371. Epub 2015/05/23. https://doi.org/10.1038/srep10371 PMID: 25996439; PubMed Central PMCID: PMC4440524.

23. Iwami S, Sato K, De Boer RJ, Aihara K, Miura T, Koyanagi Y. Identifying viral parameters from in vitro cell cultures. Frontiers in microbiology. 2012; 3:319. Epub 2012/09/13. https://doi.org/10.3389/fmicb.2012.00319 PMID: 22969758; PubMed Central PMCID: PMC3432869.

24. Perelson AS. Modelling viral and immune system dynamics. Nature reviews Immunology. 2002; 2 (1):28–36. Epub 2002/03/22. https://doi.org/10.1038/nri700 PMID: 11905835.

25. Nowak M, May RM. Virus dynamics: mathematical principles of immunology and virology: mathematical principles of immunology and virology: Oxford University Press, UK; 2000.

26. Hurtado PJ, Kirosingh AS. Generalizations of the 'Linear Chain Trick': incorporating more flexible dwell time distributions into mean field ODE models. J Math Biol. 2019; 79(5):1831–83. Epub 2019/08/15. https://doi.org/10.1007/s00285-019-01412-w PMID: 31410551; PubMed Central PMCID: PMC6800873.

27. MacDonald N, MacDonald N. Biological delay systems: linear stability theory: Cambridge University Press; 2008.

28. Mittler JE, Sulzer B, Neumann AU, Perelson AS. Influence of delayed viral production on viral dynamics in HIV-1 infected patients. Mathematical biosciences. 1998; 152(2):143–63. Epub 1998/10/22. https://doi.org/10.1016/s0025-5564(98)10027-5 PMID: 9780612.

29. Yin J, Mccaskill JS. Replication of Viruses in a Growing Plaque—a Reaction-Diffusion Model. Biophys J. 1992; 61(6):1540–9. https://doi.org/10.1016/S0006-3495(92)81958-6 PubMed PMID: WOS: A1992HZ26600009. PMID: 1617137

30. You LC, Yin J. Amplification and spread of viruses in a growing plaque. J Theor Biol. 1999; 200(4):365–73. https://doi.org/10.1006/jtbi.1999.1001 PubMed PMID: WOS:000083388900002. PMID: 10525396

31. Alvarez LJ, Thomen P, Makushok T, Chatenay D. Propagation of fluorescent viruses in growing plaques. Biotechnol Bioeng. 2007; 96(3):615–21. https://doi.org/10.1002/bit.21110 PubMed PMID: WOS:000245002600020. PMID: 16900526

32. Haseltine EL, Lam V, Yin J, Rawlings JB. Image-guided modeling of virus growth and spread. B Math Biol. 2008; 70(6):1730–48. https://doi.org/10.1007/s11538-008-9316-3 PubMed PMID: WOS:000258085500008. PMID: 18437499

33. Beauchemin C, Samuel J, Tuszynski J. A simple cellular automaton model for influenza A viral infections. J Theor Biol. 2005; 232(2):223–34. Epub 2004/11/09. https://doi.org/10.1016/j.jtbi.2004.08.001 PMID: 15530492.

34. Bauer AL, Beauchemin CA, Perelson AS. Agent-based modeling of host-pathogen systems: The successes and challenges. Inf Sci (N Y). 2009; 179(10):1379–89. Epub 2010/02/18. https://doi.org/10.1016/j.ins.2008.11.012 PMID: 20161146; PubMed Central PMCID: PMC2731970.

35. Kumberger P, Durso-Cain K, Uprichard SL, Dahari H, Graw F. Accounting for Space—Quantification of Cell-To-Cell Transmission Kinetics Using Virus Dynamics Models. Viruses-Basel. 2018; 10(4). doi: ARTN 200. https://doi.org/10.3390/v10040200 PubMed PMID: WOS:000435184400061. PMID: 29673154

36. Graw F, Balagopal A, Kandathil AJ, Ray SC, Thomas DL, Ribeiro RM, et al. Inferring viral dynamics in chronically HCV infected patients from the spatial distribution of infected hepatocytes. PLoS Comput Biol. 2014; 10(11):e1003934. Epub 2014/11/14. https://doi.org/10.1371/journal.pcbi.1003934 PMID: 25393308; PubMed Central PMCID: PMC4230741.

37. Kondoh T, Letko M, Munster VJ, Manzoor R, Maruyama J, Furuyama W, et al. Single-Nucleotide Polymorphisms in Human NPC1 Influence Filovirus Entry Into Cells. J Infect Dis. 2018; 218:S397–S402. https://doi.org/10.1093/infdis/jiy248 PubMed PMID: WOS:000460640400017. PMID: 30010949

38. Baron RC, McCormick JB, Zubeir OA. Ebola virus disease in southern Sudan: hospital dissemination and intrafamilial spread. Bull World Health Organ. 1983; 61(6):997–1003. Epub 1983/01/01. PMID: 6370486; PubMed Central PMCID: PMC2536233.

39. Dean NE, Halloran ME, Yang Y, Longini IM. Transmissibility and Pathogenicity of Ebola Virus: A Systematic Review and Meta-analysis of Household Secondary Attack Rate and Asymptomatic Infection. Clin Infect Dis. 2016; 62(10):1277–86. Epub 2016/03/05. https://doi.org/10.1093/cid/ciw114 PMID: 26932131; PubMed Central PMCID: PMC4845791.

40. Ma X, Wang H, Ji J, Xu W, Sun Y, Li W, et al. Hippo signaling promotes JNK-dependent cell migration. Proc Natl Acad Sci U S A. 2017; 114(8):1934–9. Epub 2017/02/09. https://doi.org/10.1073/pnas.1621359114 PMID: 28174264; PubMed Central PMCID: PMC5338425.

41. Mahgoub M, Yasunaga JI, Iwami S, Nakaoka S, Koizumi Y, Shimura K, et al. Sporadic on/off switching of HTLV-1 Tax expression is crucial to maintain the whole population of virus-induced leukemic cells. Proc Natl Acad Sci U S A. 2018; 115(6):E1269–E78. Epub 2018/01/24. https://doi.org/10.1073/pnas.1715724115 PMID: 29358408; PubMed Central PMCID: PMC5819419.

42. Takada A, Feldmann H, Stroeher U, Bray M, Watanabe S, Ito H, et al. Identification of protective epitopes on ebola virus glycoprotein at the single amino acid level by using recombinant vesicular stomatitis viruses. J Virol. 2003; 77(2):1069–74. Epub 2002/12/28. https://doi.org/10.1128/jvi.77.2.1069-1074.2003 PMID: 12502822; PubMed Central PMCID: PMC140786.

43. Kajihara M, Nakayama E, Marzi A, Igarashi M, Feldmann H, Takada A. Novel mutations in Marburg virus glycoprotein associated with viral evasion from antibody mediated immune pressure. J Gen Virol. 2013; 94(Pt 4):876–83. Epub 2013/01/05. https://doi.org/10.1099/vir.0.049114-0 PMID: 23288419; PubMed Central PMCID: PMC3709686.